25th ABCM International Congress of Mechanical Engineering
October 20-25, 2019, Uberlândia, MG, Brazil

COB-2019-2004
DEVELOPMENT OF A METHODOLOGY FOR SMALL SCALE CASING WEAR TESTING

Edja Iandeyara Freitas Moura
Juliano Oséias de Morais
João Pedro Costa Cardoso
Sinésio Domingues Franco
Federal University of Uberlândia
edja_moura@yahoo.com
juliano.moraes@ltad.com.br
joaopedro.mec.98@gmail.com
sdfranco@ufu.br

Joseir Granda Percy
Petrobras
joseir@petrobras.com.br

Abstract. *Casing wear is the phenomenon caused by the tribological contact of the drill string tool joint with casing. This contact causes a decrease in the thickness of the inner casing wall, weakening the structural resistance of the oil well, which can cause production stoppages and integrity failures. The API 7CW standard proposes a methodology for full-scale casing wear tests that requires considerable physical structure and material consumption. In addition to the 7CW standard, the technical literature presents mathematical models for predicting casing wear from field data. In this work we developed a methodology for small-scale casing wear test and wear mechanism evaluation. For this purpose, API 7CW, ASTM B611 -13 and NBR 13818-97 standards were used as reference. In the end, the small-scale test could be validated by comparing the wear behavior in the small-scale test with those found in the technical literature. In addition, the wear mechanisms of casing sample were analyzed Thus, the results obtained in the small-scale test may be used in the future for comparison with API 7CW tests. Moreover, this work enables the study of different hardbanding materials in a simpler way, in order to apply them in the most efficient way.*

Keywords: *casing wear; hardbanding; small scale*

1. INTRODUCTION

Oil well integrity is generally guaranteed through casings, which consist of cemented metal pipes inserted as the well is drilled, Thomas (2001). Drilling is performed by tubular elements (drill string) containing at its end a drill suitable for rock removal. The drill string is mostly made up of drill pipes (DP), which have at their ends connections with tapered threads larger than the DP body, called tool joints (TJ).

During well drilling there is contact between the drill string TJ and casing, which can lead to excessive wear of these components and removal of casing wall thickness. Casing wear (CW) can lead to loss of well integrity, making it impossible to carry out the necessary loads for construction and production. With the function of reducing CW and increasing the life of TJ, anti-wear alloys called hardbanding (HB) are deposited on the TJ. For these reasons, the CW study is relevant to industry as it enables increased reliability of structural capacity during the design phase and reduced costs in oil exploration.

Due to the exposed problems, a standard (API 7CW) was developed that proposes a wear test methodology for casing wear evaluation. Such tests are performed on a full scale and demand great use of physical structure and material consumption.

In addition to the API 7CW standard, mathematical models that analyze the quantitative parameters that determine the loss of material in the casing inner wall are found in the technical literature, seeking to predict the behavior of CW in the well. White and Dawson (1987) developed a linear casing wear model (wear-efficiency model), which correlates the volume of material lost with the energy dissipated on contact. Hall et al. (2005) presented an evolution of the theory, including the influence of limit pressure on contact. Additionally, Gao and Sun (2012) modified the wear-efficiency model considering the contact pressure variation and developed the nonlinear casing wear model.

Thus, the opportunity arises to develop a simpler and faster methodology for performing small scale tests that can reproduce the wear in the pair casing-tool joint (C-TJ). And the paper presents a study for the development of this methodology. For this, the ASTM B 611-13 standard was used as a reference for the configuration of the test procedure, equipment and sample manufacture. The maximum wear depth was calculated in three different ways: from the measurement of the wear path length, mass loss and interferometry. For the first two was used the NBR 13818-97

standard, which presents equations for the calculation of the volume of material removed in deep abrasion resistance tests.

At the end, it was found if the test configuration and the methodology developed in the small-scale tests allow simulating the field behavior predicted by the mathematical models. And the results were validated comparing the wear behavior obtained with the behavior presented by the authors Hall et al. (2005) and Sun and Gao (2012).

Additionally, a microscopic study on the worn casing area was also performed to identify the mechanism of wear. In future work, the wear mechanisms observed in this work will be compared with the wear mechanisms observed in tests performed according to API 7CW standard.

In the future, full scale assays will also be used as validators of the obtained results.

2. METHODOLOGY

2.1 Casing wear test

A cylinder-to-cylinder test configuration was used to reproduce the abrasive wear observed in the C-TJ tribological pair. For this, a test that resembles that of ASTM B611-13 has been performed. However, equipment adaptations were made and the parameters used were similar to those specified in the CW assay described by the API.

Adaptations to the equipment include the manufacture of a new HB disk holder and a cooler to keep the temperature constant at the time of testing. Regarding the test parameters, the contact pressure and the rotation speed were modified and the applied load was calculated proportionally to the contact length.

For the test, a normal force of 560 N was applied to the casing sample through a lever arm and a mass deadweight of 19.04 kg. The HB was rotated at a constant speed of 155 rpm and immersed in fluid (water) with abrasive (NBR sand, 100 mesh), in the ratio of 1 ml of water to 2 g of sand, see Fig. 1. Normal force and rotation values were based on the test parameters determined by API 7CW.

To evaluate wear, the length of the wear trail and the mass loss of the casing sample were measured throughout the test at 2.5, 5, 10, 30 and 60 minutes.

At each interruption of the test, the casing sample was removed from the equipment, washed with water and subjected to acetone immersion for 2 minutes. After cleaning, the sample was dried with compressed air and the maximum wear path length was measured with a Mitutoyo model CD-8 " AX-B caliper with a nominal range of 200 mm and a resolution of 0, 01 mm. Then the sample mass was also measured on a Shimadzu model AW220 scale with a nominal range of 220 g and a resolution of 0.0001 g.

Finally, an interferometry analysis was also performed on a CLI 2000 interferometer with an infrared laser head with a resolution corresponding to 1 µm. For maximum depth analysis, measurements were made along the wear track length.

To observe the wear mechanism, the casing sample was taken to the Zeiss Supra 40 scanning electron microscope (SEM/ FEG - Field Emission Gun) for microstructural analysis.

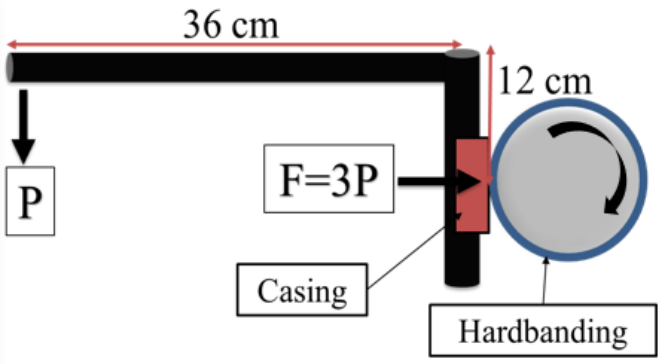

Figure 1: Scheme of the test-sample configuration

2.2 Specimen Preparation: Casing and Hardbanding

The test configuration adopted cylindrical TJ samples and flat casing samples, differing from the actual C-TJ contact configuration, which is cylinder-cylinder type. Thus, samples were manufactured following the recommendations and tolerances established by ASTM B 611-13, and were taken from a casing tube. Its dimensions were 12.7 mm (height) x 76.5 mm (length) x 25.4 mm (width).

In the manufacture of cylindrical samples, a HB commonly used in drilling components on a mechanical pipe was applied. The deposition process was the MIG / MAG. On deposition, the average layer thickness was 2 mm. The application procedure followed the technical specifications guidelines for HB applications.

After HB deposition, the disc was cut to a width of 12.8 mm. The sample underwent a grinding process on the external cylindrical surface in order to remove the non-uniformity left by the deposition process. After grinding, the HB disc had a final dimension of 156.93 mm (diameter).

2.3 Wear Calculation

The casing sample was calculated in three ways, all in search of the maximum depth caused by the cylindrical geometry of the HB. The first of these was made from geometric measurements of wear groove length, the second from mass loss measurement and finally the third from interferometry measurement.

2.3.1 Depth Calculation from Length

In calculating depth from the measurement of wear length, Equation 1 was used.

$$\sin(\alpha) = \frac{C_{cav} \cdot 2}{d} \tag{1}$$

Where C_{cav} represents the length of the wear trail over the casing sample and α corresponds to the angle formed between the disc radio that are projected at the ends of the cavity, see Fig. 2-a. After obtaining the angle α from the measured C_{cav} and the radius of the disc, it is possible to calculate the maximum depth according to Eq. 2.

Eq. 2 is given from the geometric relationship between α, β, Y and Y ', as shown in Fig. 2-a and b.

$$Y' = r - Y \tag{2}$$

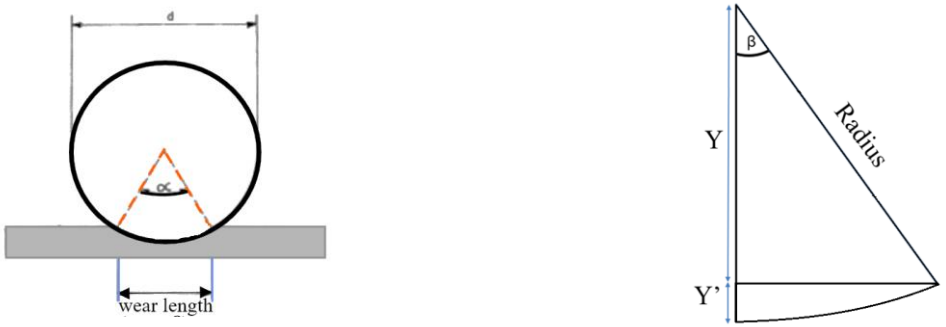

a) b)

Figure 2: Sketch of contact disc sample after wear. a) Geometric wear in casing and b) Identification of wear depth

Determining the value of angle α yields β, which represents half of the value of α. From the cosine of β, Y is calculated and then Y ', which represents the maximum depth of wear.

2.3.2 Depth Calculation from Mass Loss

For the calculation using mass measurements, the sample was weighed before and after each cycle. The material density corresponding to 7.75 g / cm³ was used to calculate the lost volume from the casing lost mass difference. Then, the angle α was calculated using Equation 3.

$$\alpha - \sin(\alpha) = \frac{8V}{hd^2} \tag{3}$$

In Eq. 3, V represents the lost volume, in mm³. h and d represent, respectively, the width and diameter of the disc, both in mm. After obtaining the angle α, the maximum wear depth is also calculated from Eq. 2 and the trigonometric relations already mentioned.

2.3.3 Depth Calculation from Interferometry

In interferometry measurement, depth was measured along the length of the wear path, initially from the centerline (CL), as shown in Fig. 3. Then two other measurements were made, one moving the reading line 2 mm to the right of the center line and the other 2 mm to the left of it. In this method, the average value of the three measurements for determining the depth of wear.

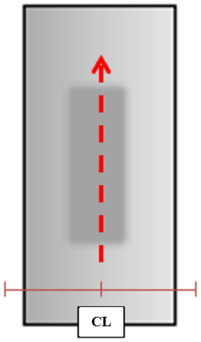

Figure 3: Schematic drawing of the region where depth was measured from interferometry

3. RESULTS AND DISCUSSION

After the tests were performed, the predicted wear calculations were made. Fig. 4-a presents a graph showing the variation in wear depth according to the test time for the three measurement methods (from length, from mass loss and from interferometry). Analyzing the behavior of curve 1, obtained from the length, it can be observed that the maximum depth calculated by this method resulted in 0.88 mm. In curve 2, obtained from the mass loss, the maximum depth resulted in a value of 0.41 mm (54% smaller). Curve 3 represents the interferometry measurement. In Fig. 4-b, one of the profiles measured at the end of the test, indicating a final depth of 0.3567 mm.

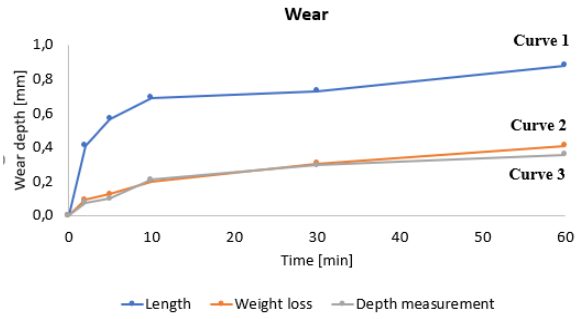

a)

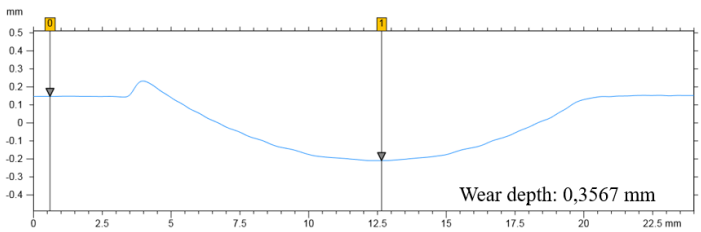

b)

Figure 4: a) Depth wear graph over time for the three measurement methods and b) Profile along the wear track obtained by interferometry at the end of the test.

The method of measuring track length with the caliper was the most inaccurate, and it can be misleading since defining exactly where the beginning and end of the track is a naked eye analysis, see Fig. 5-a and Fig. 5-b. However, it was considered to be the simplest of them and, if it presented results with low errors, could be adopted to measure wear with the sample mounted on the equipment. However, the results obtained with this measurement technique showed great inaccuracy in relation to the other techniques.

a)

b)

Figure 5: a) Worn surface of casing sample and b) Measurement of wear track length from caliper.

The cause of this large measurement difference stems from several errors that are intrinsic to depth measurement and calculation. In the case of measurement from length, the inaccuracy of the wear reading may be linked to the setting

of the start and end of the wear track as well as the parallax error, which is caused by a shift in the operator's viewing angle.

For depth measurement from length as well as depth measurement from mass loss, calculations according to NBR 13818-97 are used to determine the maximum depth of wear. These calculations considered that the geometric shape of the groove is identical to that of the surface of the HB disc that promoted the wear. However, this geometry is not perfectly cylindrical.

Measurement from interferometry, curve 3 of Fig. 4-a, is the most accurate since it directly measures the desired quantity, becoming the most appropriate among the methodologies analyzed. The result of this analysis showed a maximum depth of approximately 0.35 mm. See Fig. 4-b.

Comparing the results, it was found that, among the calculation methods mentioned in this article, the calculation of wear from the length measurement with the caliper, although simple, is not applicable because it is subject to major errors, due to the appearance wear on the surface of the sample. Otherwise, wear calculated from mass loss is a good method for direct comparison of materials, however it has a final error of 17% when used to find the maximum depth, considering the measured value on the interferometer as a reference value. In other words, the methods in which calculations are used present errors that do not allow their use to evaluate the maximum wear depth, while the interferometric measurement is appropriate to determine this parameter.

Comparing the behavior of the results obtained in a small-scale test with the behavior of the results presented in the literature from the mathematical models, see Fig. 6, it is found that the variation of wear depth over time is similar in all three cases. Therefore, the adopted configurations do not seem to significantly affect the wear behavior over time.

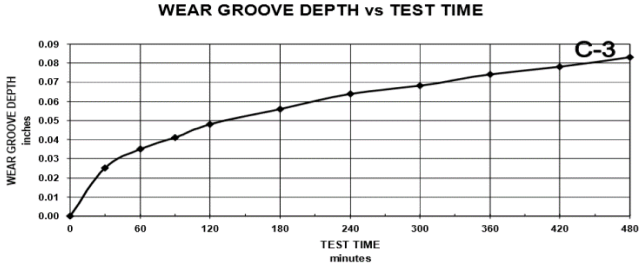

Figure 6: Graph of the evolution of wear depth as a function of time proposed by Hall et al. (2005) in tests according to the API.

Thus, the calculation method used for the determination of wear in small-scale tests can validly provide useful information for comparing field situations. In fact, the behavior of the graph in Fig. 4-a, developed from the calculation method proposed in this article, is similar to the wear behavior predicted by the authors Hall et al. (2005).

3.1 Wear Mechanism

Analyzing the sample with naked eyes, after 2.5 minutes of testing (Fig. 6-a), we can see two regions with different aspects, one located in the central region of the groove and the other in the upper and lower regions. A microscopic analysis of the worn surface with closer approximation shows the predominance of metal-to-metal sliding contact in the central region and the occurrence of abrasion in the upper and lower portions, Fig. 6-b and c. The yellow arrows in the upper left corner of each figure indicate the sliding direction of the disc.

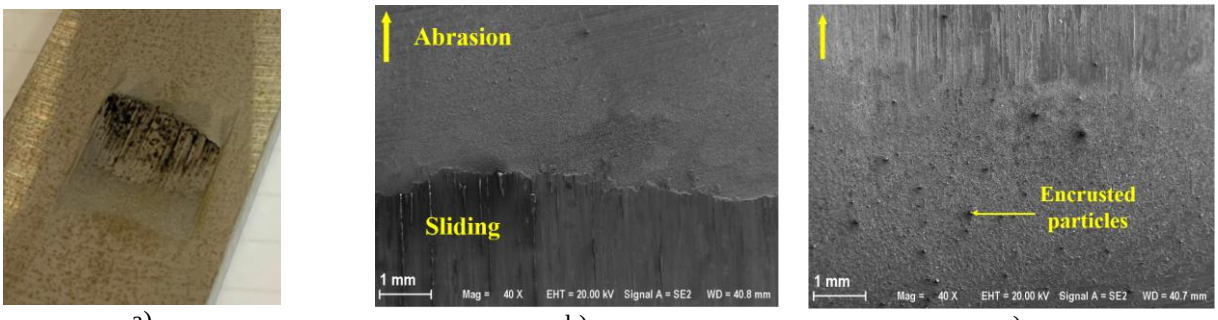

a) b) c)

Figure 6: Analysis of the worn surface of the casing sample, time of 2.5 minutes. a) Macroscopy of wear; b) SEM of the upper region and c) SEM of the lower region.

Fig. 7-a shows, with greater approximation, the interface between the degradation mechanisms, where large plastic deformation is observed moving material from the central part to the upper part of the wear.

Fig. 7-b, obtained in the central region, shows, more clearly, how the sliding mechanism acts on casing wear, with little action of the abrasive groove wear mechanism. In Fig. 7-c it is possible to see the morphology of this part of the

worn surface in more detail. It shows plastic deformation and the emergence of cracks that favor the removal of material. Still in Fig. 7-c we see bow formation marks, characteristic feature of the groove, which is less frequent.

According to Hutchings (1992), the typical damage of sliding wear would be dragging and grooves, the former occurring in non-lubricated metal contact.

Observing Fig. 7-d, referring to the bottom, predominates the abrasive degradation caused by indentations of the abrasive particles present in the fluid. In Fig. 7-e, one can see in detail the surface-encrusted particles due to the mentioned mechanism, which occurs when the abrasive particle touches the surface with a certain load but without slipping, generates localized plastic deformation, Hutchings (1992).

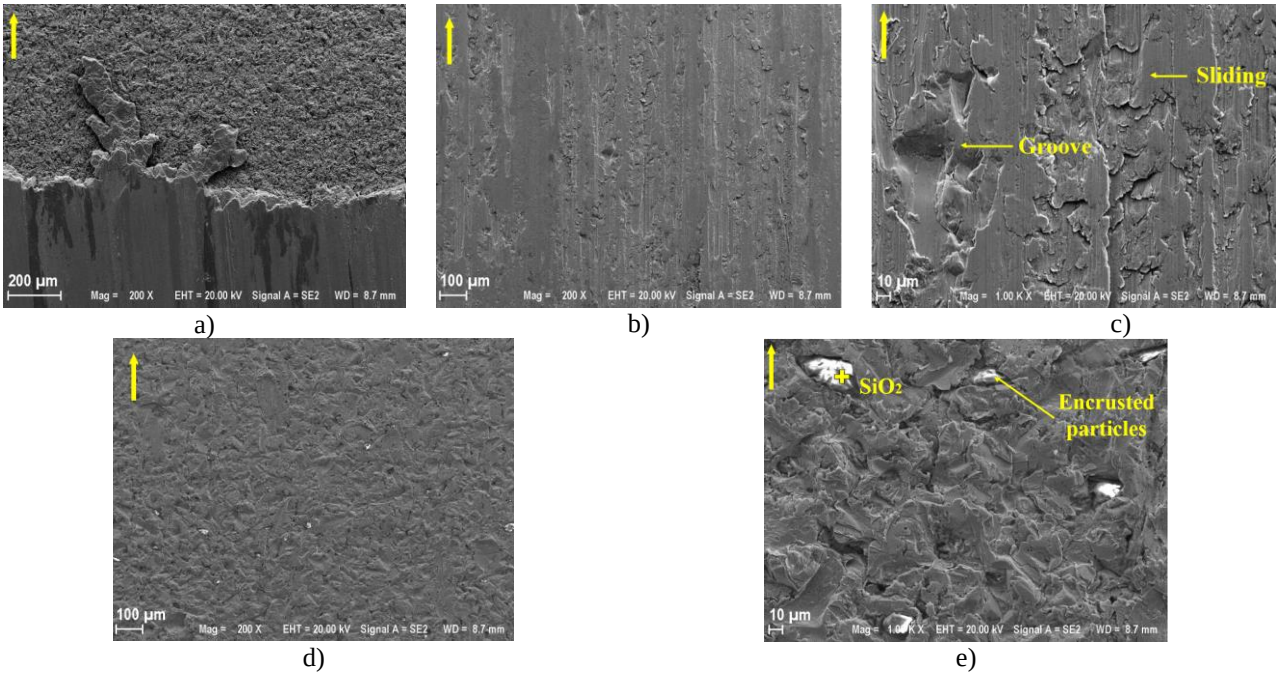

Figure 7: Investigation of wear micromechanisms. a) SEM of the interface between central and upper region; b) SEM of the central region; c) detail of the image b; d) SEM of the lower region; and e) image d detail. The yellow arrows in the upper left corner of each figure indicate the sliding direction of the disc.

At the end of the test, after 60 minutes, as shown in Figs. 8-a, b and c, the same initial degradation mechanisms were observed. However, the area of sliding wear increased, and it can be said that the already predominant metal-to-metal slip became even more pronounced in relation to abrasion. With a smaller approximation, Fig. 8-b shows the metal slip from the central region to the upper region, maintaining the same behavior at the interface when compared to the beginning of the test. Fig. 8-c shows the surface degradation still showing indentation abrasion marks with encrusted particles on the surface. This behavior happens only at the beginning and end of the wear track and has been verified since the initial phase of the test.

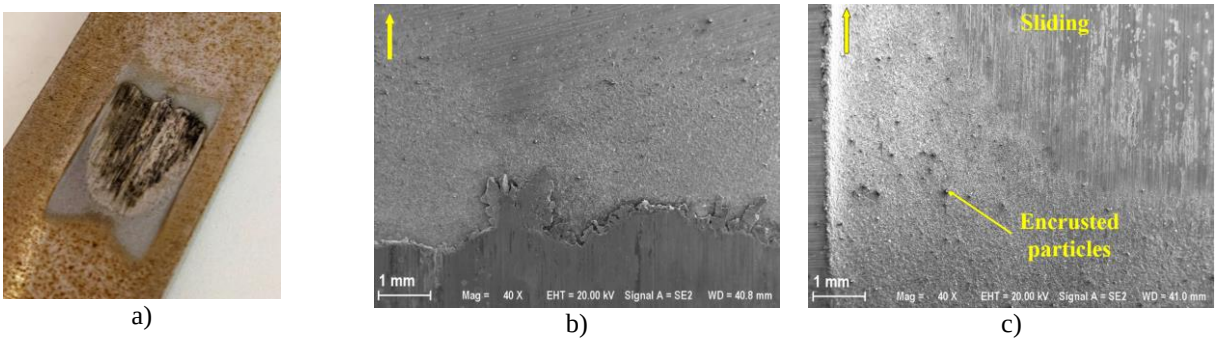

Figure 8: Worn surface analysis of casing sample, time 60 minutes. a) Macroscopy of wear; b) SEM of the upper region and c) SEM of the lower region

Figs 9-a, b, c, d and e also show more closely the regions of wear. Even with increased wear area and consequent decrease in contact pressure, severe plastic deformation causing cracks transverse to the wear direction was still observed, see Fig 9-c.

Fig. 9-d and Fig. 9-e, corresponding to an increase of the former, show the interface between abrasion and sliding, respectively, in the lower region and in the central region. In this area, one can see characteristic groove marks, indentations and the slip resulting from metal-to-metal contact.

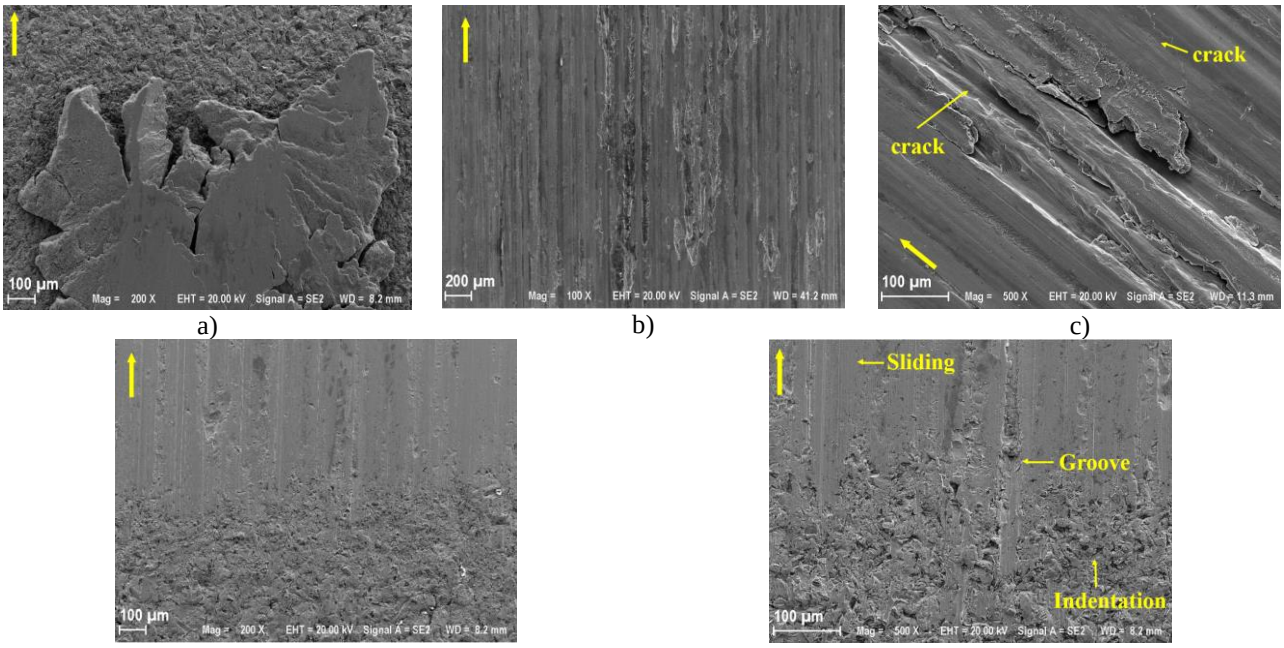

a) b) c)

d) e)

Figure 9: Investigation of wear micromechanisms. a) SEM of the upper region; b) SEM of the median region; c) SEM of the lower region; d) detail of the plastic deformation suffered on the surface and e) detail of the image c.

The images in Fig. 9 confirm the occurrence of slip and abrasion degradation mechanisms, with surface degradation due to material slip being predominant. Also, in Fig. 4-b, concerning the interferometry analysis performed in the casing sample in 60 minutes time, it is possible to identify, macroscopically, the lifting of a bow of material in the direction of sliding of the disc.

4. CONCLUSION

In the present study, it was found that a small-scale test for wear analysis of the C-TJ pair can be developed from ASTM B611-13, API 7CW and NBR 13818-97 standards. Three alternatives for measuring and calculating wear depth were presented, one from groove length measurement, one from mass loss measurement, and the last from direct interferometry depth measurement. The latter proved to be more appropriate because its results do not involve calculation errors, being dependent only on the resolution of the equipment during the measurement.

Another important result concerns the comparability of the wear behavior of the small-scale tests with the wear behavior of the mathematical models presented in the literature. From the graphical comparison performed, it was possible to validate the small-scale assay.

Regarding the evaluation of surface wear, it was verified the predominance of the sliding degradation mechanism in face of the indentation and groove abrasive wear mechanism. In a future study, this result will be compared with the wear mechanisms caused by the full-scale test conditions provided by API 7CW.

In conclusion, the present work presents a simpler but valid methodology to quantify and compare the wear caused by different HBs, making it possible to rank them and apply them in the oil and gas industry in a more efficient way.

5. REFERENCES

Archard, J., Wear theory and mechanisms. In Peterson, M., Winer, W. (Eds.), Wear control handbook. American Society of Machanical Engineers, New York. p 35-80, 1980.

AMERICAN PETROLEUM INSTITUTE. **Casing Wear Teste**. API 7CW. 1 ed. Jun, 2015;

AMERICAN SOCIETY FOR TESTING AND MATERIALS. **Standard Test Method for Determining the High Stress Abrasion Resistance of Hard Materials.** West Conshohocken. ASTM B611-13, 15 ed., Jun 2016.

ASSOCIAÇÃO BRASILEIRA DE NORMAS TÉCNICAS. **Placas cerâmicas para revestimento – Especificação e métodos de ensaios**. NBR 13818-97. Abr, 1997.

Gahr, K. Z; Microstructure and ear of Materials. Tribology Series, vol. 10. Elsevier Science Publishers B.V. Amsterdam, 1ª edição, ISBN-13: 978-0444427540, 560 p, 1987.

Gao, D.; Sun, L.;New Methodo for predicting casing wear in horizontal drilling. **Petroleum Science and Technology.** 30:9 p. 883-892, 2012; DOI: 10.1080/10916466.2010.493909;

Hall K.P., R. W. M. Contact Pressure Threshold: An Important New Aspect of Casing Wear. **Society of Petroleum Engineers**, v. SPE 9430, p. 1–7, 2005.

Hall, R. W. et al. Recent Advances in Casing Wear Technology. 1994.

Hutchings, I. M. "Tribology: Friction and Wear of Engineering Materials"; CRC Press, Boca Raton, USA, ISBN-13: 978-0340561843, 273 p, 1992.

Thomas, J. E., Fundamentos de Engenharia do Petróleo, editora Interciência, 2º edição, Rio de Janeiro, 2001, 271 p.

White, J. P. and Dawson, R., Casing Wear: Laboratory Measurements and Field Prediction. **Society of Petroleum Engineer**, p. 56-62, 1987.

6. ACKONWLEDGMENT

Petrobras, CAPES and the FEMEC at the Federal University of Uberlândia

7. RESPONSIBILITY NOTICE

The five authors are the only responsible for the printed material included in this paper.